We are IntechOpen, the world's leading publisher of Open Access books
Built by scientists, for scientists

5,000
Open access books available

125,000
International authors and editors

140M
Downloads

Our authors are among the

154
Countries delivered to

TOP 1%
most cited scientists

12.2%
Contributors from top 500 universities

BOOK CITATION INDEX
CLARIVATE ANALYTICS
INDEXED

WEB OF SCIENCE™

Selection of our books indexed in the Book Citation Index
in Web of Science™ Core Collection (BKCI)

Interested in publishing with us?
Contact book.department@intechopen.com

Numbers displayed above are based on latest data collected.
For more information visit www.intechopen.com

Structural, Electrical, and Magnetic Properties of Mullite-Type Ceramic: Bi$_2$Fe$_4$O$_9$

Poorva Sharma, Ashwini Kumar, Jingyou Tang and Guolong Tan

Abstract

This work reports the structure, electrical and magnetic properties of the orthorhombic (*Pbam*) structured bulk Bi$_2$Fe$_4$O$_9$ synthesized by the solid-state reaction process. Bi$_2$Fe$_4$O$_9$ has been studied using several experimental techniques such as X-ray diffraction, scanning electron microscopy, Raman spectroscopy, dielectric spectroscopy, and magnetometry. Rietveld-refined X-ray diffraction data and Raman spectroscopy results clearly reveal the formation of Bi$_2$Fe$_4$O$_9$ perovskite structure and all the peaks of Bi$_2$Fe$_4$O$_9$ perfectly indexed in the orthorhombic (*Pbam*) structure. It has been established that the Raman spectrum identified A$_g$, B$_{2g}$, and B$_{3g}$ active optical phonon modes, and that the Raman peak at 470 cm^{-1} may have a magnetic origin. As a result, the coexistence of weak ferromagnetic and antiferromagnetic orders in Bi$_2$Fe$_4$O$_9$ ceramic was established. The remanent magnetization (2M_r) and coercivity (2H_c) are 8.74 × 10^{-4} emu/g and 478.8 Oe, respectively. We report a remarkable multiferroic effects in polycrystalline Bi$_2$Fe$_4$O$_9$ ceramic. These characteristics make this material very useful in technology and practical applications.

Keywords: multiferroic, Bi$_2$Fe$_4$O$_9$, Raman spectroscopy, ferroelectric, magnetic measurement

1. Introduction

Multiferroic materials exhibit more than one primary ferroic order parameters (i.e. ferroelectricity, ferroelasticity and ferromagnetism) in same phase which was first proposed by Schmid in 1994 [1]. In recent years, there has been a strong interest in systems that exhibit convergence between magnetic degrees of freedom, electronic degrees of freedom, and orbital degrees of freedom. Perovskite based oxides have attracted much attention due to their interesting structural, magnetic, optical and electronic properties [2]. A large number of publications have been devoted to multiferroic materials working with theory, experimentation and application features. Bismuth-based complex oxides (Bi$_2$Fe$_4$O$_9$) with mullite-type structure, as an important active material, has a wide application prospect in the fields of magnetic recording media, sensor, magnetoresistive devices, solid oxide fuel cell, scintillators and photocatalyst [3–7].

The crystallographic structure of Bi$_2$Fe$_4$O$_9$ is orthorhombic with space group *Pbam*, No. 55, which belongs to the mullite-type crystal structure family [8, 9].

A unit cell of $Bi_2Fe_4O_9$ consists of two formula units with an equal distribution of Fe ions between the edge-sharing octahedral (FeO_6) and corner-sharing tetrahedral (FeO_4) positions with Bi^{3+} ions are surrounded by eight oxygen atoms. Bulk $Bi_2Fe_4O_9$ synthesized by solid state reaction exhibiting an antiferromagnetic (AFM) ordering at T_N = 260 K and ferroelectric (FE) hysteresis loops at T = 250 K, which indicates that $Bi_2Fe_4O_9$ is a promising multiferroic material [9, 10]. An unexpected multiferroic effect, which was observed as a coexistence of AFM and FE polarization, was reported in $Bi_2Fe_4O_9$, attributed to frustrated spin system coupled with phonons [10]. Low electrical conductivity in ferrites is useful for inductor, transformer cores and in switch mode power supplies. On the other hand, studies of electric and dielectric properties are also equally important from both fundamental and application point of view. Dielectric and magnetic behavior of ferrites is greatly influenced by an order of magnitude of conductivity and is mostly dependent on preparation method and sintering conditions [11].

Although, due to search of new multifunctional materials, the recent work carried out is the very important and needed [12–15]. Rao et al. reported the multifunctional properties of mullite-type structured Nd-doped $Bi_2Fe_4O_9$ and the spin-orbital coupling by D-M interactions enhances the ferromagnetic (FM) behavior of the Nd-doping $Bi_2Fe_4O_9$ [12]. Ameer et al. studied the structural, electronic, and magnetic properties of $Bi_2Fe_4O_9$ with different magnetic ordering using the projector augmented wave (PAW) method based on density functional theory (DFT). They proposed that the FM $Bi_2Fe_4O_9$ is a semiconductor with an indirect optical bandgap of 1.732 eV and the exchange mechanism started to work, resulting in the exchange splitting in $Bi_2Fe_4O_9$, while the antiferromagnetic (AFM) $Bi_2Fe_4O_9$ is a multiband semiconductor without splitting of the majority and minority spin states [13]. In another study, the researchers believed that Zn substitution in $Bi_2Fe_4O_9$ would induce p-type conductivity, suggesting that $3d$ transition metal ions doping in $Bi_2Fe_4O_9$ provides the capabilities to develop low-bandgap, heterojunction-based optoelectronic devices [14]. In addition, Pooladi et al. studied the $Bi_2Fe_{4-x}Mn_xO_9$ ($0.0 \leq x \leq 1.0$) nanoparticles synthesized by reverse chemical co-precipitation method. With increase in Mn concentration, the coercivity of the nanoparticles enhances significantly and the saturation magnetization decreased. Also, the Mn substitution at Fe site in $Bi_2Fe_{4-x}Mn_xO_9$ increases the dielectric constant [15]. These types of structures and materials are interested due to their structural, magnetic properties and the relationship between orbital, spin and charge degrees of freedom.

Various chemical methods such as solid-state reaction route, chemical co-precipitation, sol-gel and hydrothermal have been used to produce $Bi_2Fe_4O_9$ [14–16]. The properties of materials are highly dependent on structural, microstructural properties and methods of synthesis. In this regard, it is of interest to develop controlled methods for making materials in oxide forms for further functional applications. Thermal heating in the oxygen atmosphere at high temperatures contributes to the oxidation process and formation of oxide forms, which has a significant impact on physical, chemical and magnetic properties of compounds [17–21]. Zdorovets et al. reported the systematic study of the effect of thermal annealing on changes in the structural properties and phase compositions of metallic cobalt based nanostructures [17]. Rusakov et al. described the effect of thermal annealing on structural and magnetic characteristics, as well as phase transformations in Fe–Ni/Fe–Ni–O nanoparticles. They found that the initial nanoparticles were a three-phase system consisting of Fe–Ni–O oxide with spinel structure and a Fe–Ni alloy with face-centered and body-centered cubic lattices. As a result of thermal annealing, the decrease in the Fe–Ni phase is associated with the subsequent ordering of the Fe–Ni–O phase with a decrease in the crystal lattice parameter and an increase in the degree of crystallinity [19]. If annealing is carried out in air, the phase transition

related to the structural transformation of iron oxide is in the range of 600–1000°C due to the change of thermal vibration of atoms in the lattice node, the annealing of point defects and the introduction of oxygen at high temperature [20].

Although Bi$_2$Fe$_4$O$_9$ has obvious importance as a functional material, there are few reports in the literature. Here, we present the structural and physical properties of bulk Bi$_2$Fe$_4$O$_9$ ceramic synthesized by a solid-state reaction route. One needs detailed knowledge of the crystal structure to understand the physical properties. Therefore, we aimed to understand the crystal structure by X-ray powder diffraction followed by Rietveld refinement using FullPROF program [22]. In addition, Bi$_2$Fe$_4$O$_9$ was subsequently characterized using several experimental techniques, such as Raman spectroscopy, SEM, dielectric and ferroelectric spectroscopy, and magnetometry, which are discussed in detail.

2. Experimental details

Bulk Bi$_2$Fe$_4$O$_9$ ceramic was synthesized through solid-state reaction route (SSR). The SSR is a commonly used synthesis method for obtaining polycrystalline bulk materials from solid reagents. This method provides a great deal of choices for starting materials like oxides, carbonates, etc. Since solids do not react with each other at room temperature, very high temperatures are usually employed to allow appropriate reaction to occur at a significant rate. Therefore, both thermodynamic and kinetic factors are important in SSR. In the SSR method, the solid reactants undergo a chemical reaction at high temperature in the absence of any solvent, thereby producing a stable product. High purity Bi$_2$O$_3$, Fe$_2$O$_3$ were carefully weighed and stoichiometrically mixed in an agate mortar for 5 hours. The powder was doubly thermally calcined consecutively at 650°C for 1 hour and 850°C for 6 hours with intermediate grinding in oxygen-containing medium. Finally, pellets were sintered at 850°C for 6 hours, resulting in good densification. Thermal heating (i.e. calcination and annealing) is a mean of controlling the structural changes, properties, and phase compositions [23]. In this case, introduction of oxygen leads to the formation of oxide compounds. For crystallinity and phase identification X-ray diffraction (XRD) pattern were taken using CuKα1 radiation (λ = 1.5406 Å) of a Bruker D8 Advance X-ray diffractometer. Crystal structure characterization of synthesized sample was performed by employing Rietveld whole profile fitting method using FullPROF software [22].

The sample quality, morphology, grain distribution, density/voids in the samples were studied with scanning electron microscope (JEOL, JSM-5600). Raman measurements on as synthesized sample was carried out on Jobin-Yovn Horiba LABRAM (System HR800) spectrometer with a 632.8 nm excitation source equipped with a Peltier cooled CCD detector. Dielectric measurements were made as a function of frequency in the range of 100 Hz–1 MHz on Novocontrol alpha-ANB impedance analyzer at room temperature. Ferroelectric measurement was carried out using a ferroelectric loop tracer based on Sawyer-Tower circuit. The *M-H* curve was performed using a Lakeshore VSM 7410 model.

3. Results and discussion

3.1 Crystal structure analysis

The room temperature XRD pattern of bulk Bi$_2$Fe$_4$O$_9$ sample is shown in **Figure 1(a)**. From the XRD pattern we can index the data in orthorhombic phase as shown in **Figure 1(a)**. The present XRD patterns matches with JCPDS
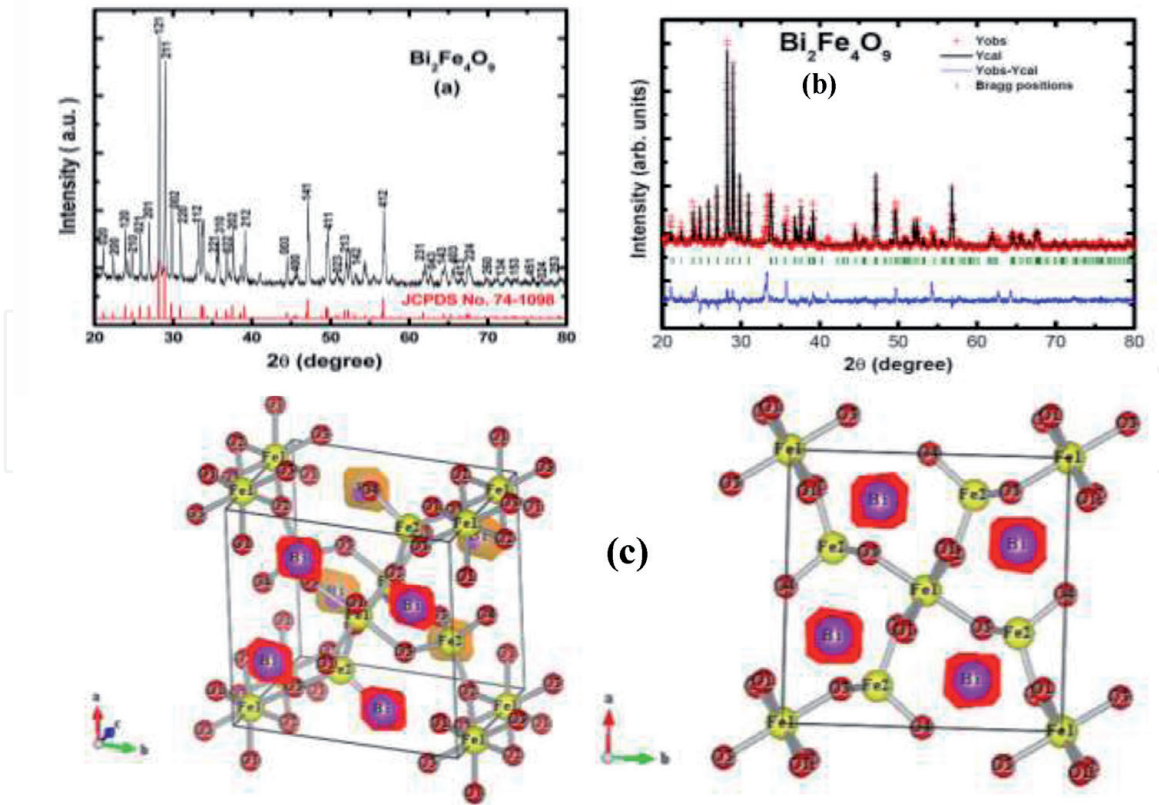
Figure 1.
(a) Measured powder X-ray diffraction pattern for Bi₂Fe₄O₉ ceramic at room temperature, (b) Rietveld-refined XRD pattern for Bi₂Fe₄O₉, and (c) symmetric representation of the unit cell for Bi₂Fe₄O₉ ceramic viewed in abc *and* ab *planes.*

#01-74-1098 ($Bi_2Fe_4O_9$) [24]. In order to further confirm structural data, Rietveld refinement of the XRD pattern for $Bi_2Fe_4O_9$ sample was performed using FullPROF program and shown in **Figure 1(b)**. The composition of phase and its concentration in the structure have been determined using the Rietveld method, which is based on the estimation of the diffraction peak area and the analysis of their contributions to the entire X-ray diffraction. It should be noted here that XRD pattern having a small secondary phase peaks corresponding to the Fe_2O_3 and its phase concentration is less than 2%, which does not affect the measured properties of studied ceramic. The XRD pattern of parent $Bi_2Fe_4O_9$ was refined with orthorhombic (*Pbam*) structure with lattice parameters a = 7.941(4) Å, b = 8.420(4) Å and c = 5.986(4) Å. The obtained lattice parameters are consistent with earlier reported data [25]. The Rietveld-refined calculated parameters of $Bi_2Fe_4O_9$ are documented in **Table 1**. We have illustrated structural parameters for $Bi_2Fe_4O_9$ ceramic, and also identify the residuals for weighted pattern R_{wp}, the expected weighted profile factor R_{exp}, and goodness of fit χ^2. The selected bond lengths and bond angles are mentioned in **Table 1**. The average value of the Bi—O bond is 2.482 Å. The generated orthorhombic structure of $Bi_2Fe_4O_9$ ceramic is depicted in **Figure 1(c)**. In the crystal structure, chains of FeO_6 octahedra parallel to the *c* axis are connected *via* FeO_4 tetrahedra alternating with bismuth atoms along the *c* axis.

The symmetric pseudo-Voigt functions are used to calculate the degree of crystallinity based on the estimation of the diffraction width and shapes. We have measured the full width half maxima (FWHM) of the recorded diffraction lines, which allowed us to characterize the perfection of the crystal structure and evaluate the degree of crystallinity [21]. The value of % of crystallinity for $Bi_2Fe_4O_9$ = 81.3% was calculated using the formula:

$$Crystallinity = \frac{Area\ of\ Crystalline\ peaks}{Area\ of\ all\ peaks\ (i.e\ Crystalline + Amorphous)} \times 100 \quad (1)$$

The *distortion of the crystal lattice* (ρ_{dil}), which characterizes the number of defective or porous inclusions in the structure as a result of external influences, was found according to formula:

$$\rho_{dil} = \left(1 - \frac{\rho}{\rho_o}\right) \times 100\% \quad (2)$$

Here, ρ_0 is the density of the reference sample taken from the JCPDS #01-74-1098 database, ρ is the calculated density of the sample. Calculated value of distortion of the crystal lattice is $\rho_{dil} = 3.1\%$.

We used the Williamson-Hall plot to observed the effect of the phase composition on distortions and deformation of the crystal structure of $Bi_2Fe_4O_9$ ceramic, based on estimating the angular dependence of the full width at half maximum (FWHM) of diffraction lines (**Figure 2**). We obtained the strain (ε) value for

$a = 7.941(4)$ Å		$b = 8.420(4)$ Å		$c = 5.986(4)$ Å	$V = 400.31(2)$ Å³
Atoms	x	y		z	**R-values**
Bi	0.3230	0.1745		0.0000	$R_{wp} = 7.36\%$
Fe₁	0.0000	0.0000		0.2582	$R_{exp} = 3.41\%$
Fe₂	0.1465	0.3360		0.5000	$R_p = 4.61\%$
O₁	0.3485	0.4292		0.0000	$\chi^2 = 4.65\%$
O₂	0.3671	0.4047		0.5000	$GoF = 2.2$
O₃	0.1312	0.2054		0.2413	
O₄	0.0000	0.5000		0.5000	
Bond type	**Bond length (Å)**		**Bond type**		**Bond angle (°)**
Bi–O₁	2.153		O₁–Bi–O₁		151.93
Bi–O₃	3.017		O₃–Bi–O₃		86.06
Fe₁–O₁	2.047		Bi–O₁–Bi		141.13
Fe₁–O₂	1.962		O₂–Fe₂–O₃		103.98
Fe₁–O₃	2.022		O₃–Fe₂–O₃		108.93
Fe₂–O₁	3.485		O₃–Fe₂–O₄		113.59
Fe₂–O₂	1.846		Fe₁–O₁–Fe₁		98.02
Fe₂–O₃	1.901		Fe₁–O₂–Fe₁		94.99
Fe₂–O₄	1.805		Fe₁–O₂–Fe₂		129.72
			Fe₁–O₃–Fe₂		119.09
			Fe₂–O₄–Fe₂		172.00

Table 1.
Rietveld-refined room temperature structural parameters, important bond lengths, and bond angles for Bi₂Fe₄O₉ ceramic from XRD.

Figure 2.
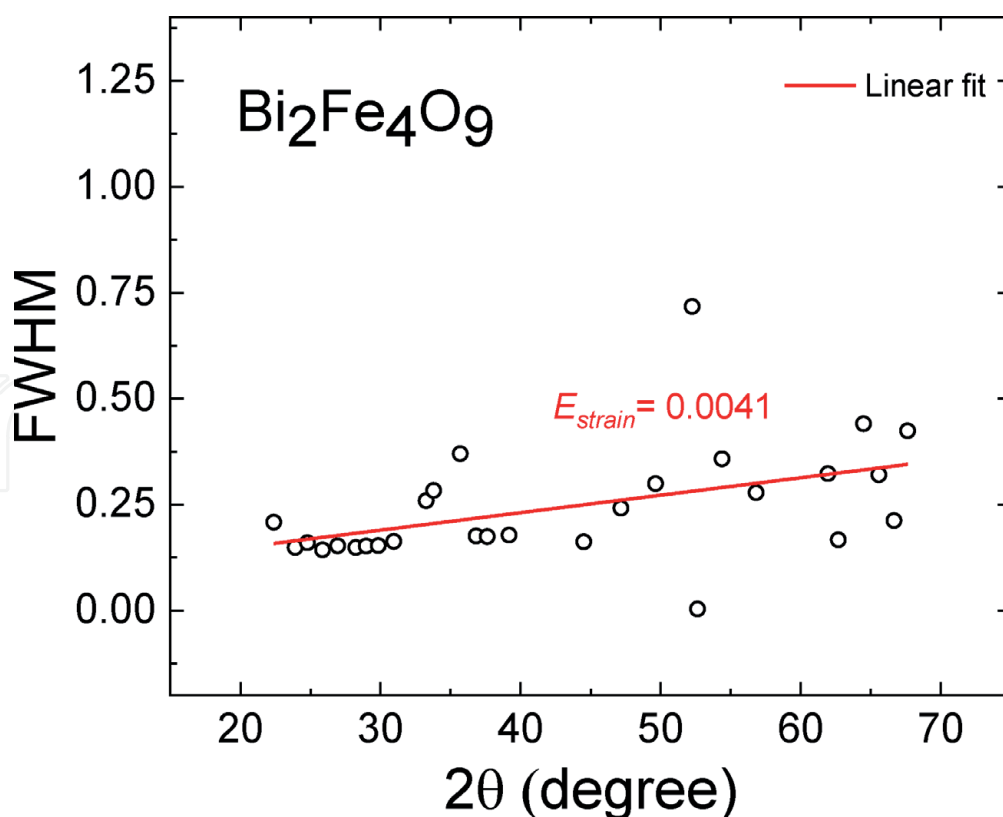*Williamson-Hall plot for Bi$_2$Fe$_4$O$_9$ ceramic.*

Bi$_2$Fe$_4$O$_9$ ceramic is 0.00412 ± 0.0016. Thermal heating at high temperature helps to reduce the distortion value [19].

3.2 SEM analysis

The surface morphological and microstructural properties of Bi$_2$Fe$_4$O$_9$ compound was investigated using scanning electron microscopy (SEM). **Figure 3** (upper part) shows the SEM micrograph of Bi$_2$Fe$_4$O$_9$ thermally sintered at 850°C for 10 hours. Typical SEM image shows that microstructures comprising of non-uniform distribution of grains with an estimated average grain size of 1.5 μm indicating polycrystalline nature. Even though the SEM image shows that there are some pores between loosely connected grains in the sample. The surface area of a catalyst is a key aspect to determine the adsorption capacity of reactants on the catalyst surface [26]. We have measured the active surface area using a Brunauer-Emmett-Teller (BET) measurement system at 77 K through nitrogen adsorption-desorption isotherm method. The BET active surface area of Bi$_2$Fe$_4$O$_9$ is 1.2 m^2/g, which is in good agreement with the values reported in the literature [27]. In order to obtain photocatalytic efficiency, it is necessary to increase the specific surface area by doping or reducing grain sizes. In addition, we have measured the material's apparent density which is defined as the mass per unit volume of the material in absolute dense condition [28]. The obtained density of the present calcined Bi$_2$Fe$_4$O$_9$ ceramic is 6.51 g/cm^3 which match well with the density for the Bi$_2$Fe$_4$O$_9$ (ρ = 6.48 g/cm^3) from reference file: JCPDS card number 74-1098.

3.3 Raman scattering analysis

Raman scattering spectroscopy has been extensively utilized to study the crystal lattice vibrations. Raman scattering spectroscopy would also offer a distinctive
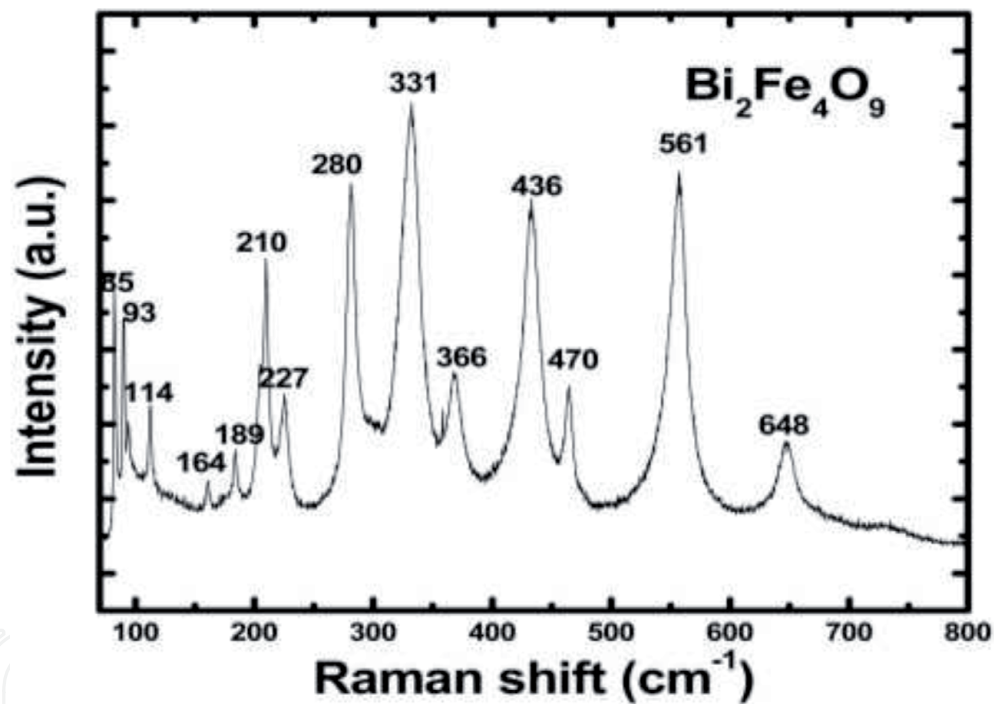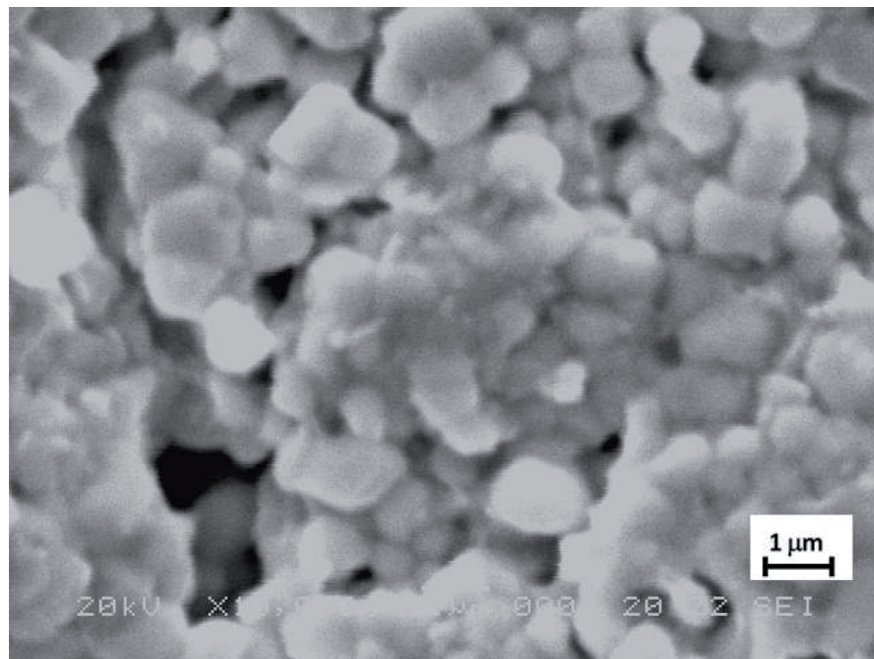
Figure 3.
(Upper) Scanning electron microscope images of Bi₂Fe₄O₉ and (lower) Raman spectra for Bi₂Fe₄O₉ mullite-type ceramic carried out at room temperature.

potential as a sensitive probe for the spin dynamics and studying the effect of magnetic ordering. Raman spectrum of $Bi_2Fe_4O_9$ at room temperature is depicted in lower part of **Figure 3**. The Raman active modes of the structure can be summarized using the irreducible representation $12A_g + 12B1_g + 9B2_g + 9B3_g$, which is employed to describe Raman modes of orthorhombic (*Pbam* space group) [9]. In the measured Raman spectra all are the A_g modes (85, 93, 114, 210, 227, 280, 331, 366, 436, 465, 561, and 648 cm^{-1}) accept modes in attendance at 164 (B_{2g}) and 189 (B_{3g}) cm^{-1}. The agreement between experimental and predicted values is relatively good for the all frequency modes, dominated by Bi vibrations. The Raman peak centered at 470 cm^{-1} is might be attributed to magnetic ordering effect on phonon line width consistent with earlier observation of bands at ~260 and 472 cm^{-1} due to

magnon scattering [9]. It would be more practical to study the magnetic excitations in $Bi_2Fe_4O_9$ under the assumption that they involve two-magnon processes, like in the well-known cases of ferrites [29] or cuprates [30, 31]. At higher frequency (>250 cm^{-1}), it is unlikely the magnetic-order-induced bands correspond to one-magnon excitations but in rare-earth orthoferrites ($RFeO_3$; R = Dy, Ho, Er, Sm, etc.) have frequencies below 25 cm^{-1} for comparison the zone-center magnons [32].

3.4 Dielectric and P-E loop studies

The real part of permittivity (ε') and loss tangent ($\tan\delta$) as a function of frequency of $Bi_2Fe_4O_9$ ceramics near at surrounding temperature is shown in **Figure 4(a)** and **(b)**. The value of ε' and $\tan\delta$ for $Bi_2Fe_4O_9$ are about 21.57 and 0.05, respectively at frequency 10 Hz. At higher frequency (~1 MHz) the value of

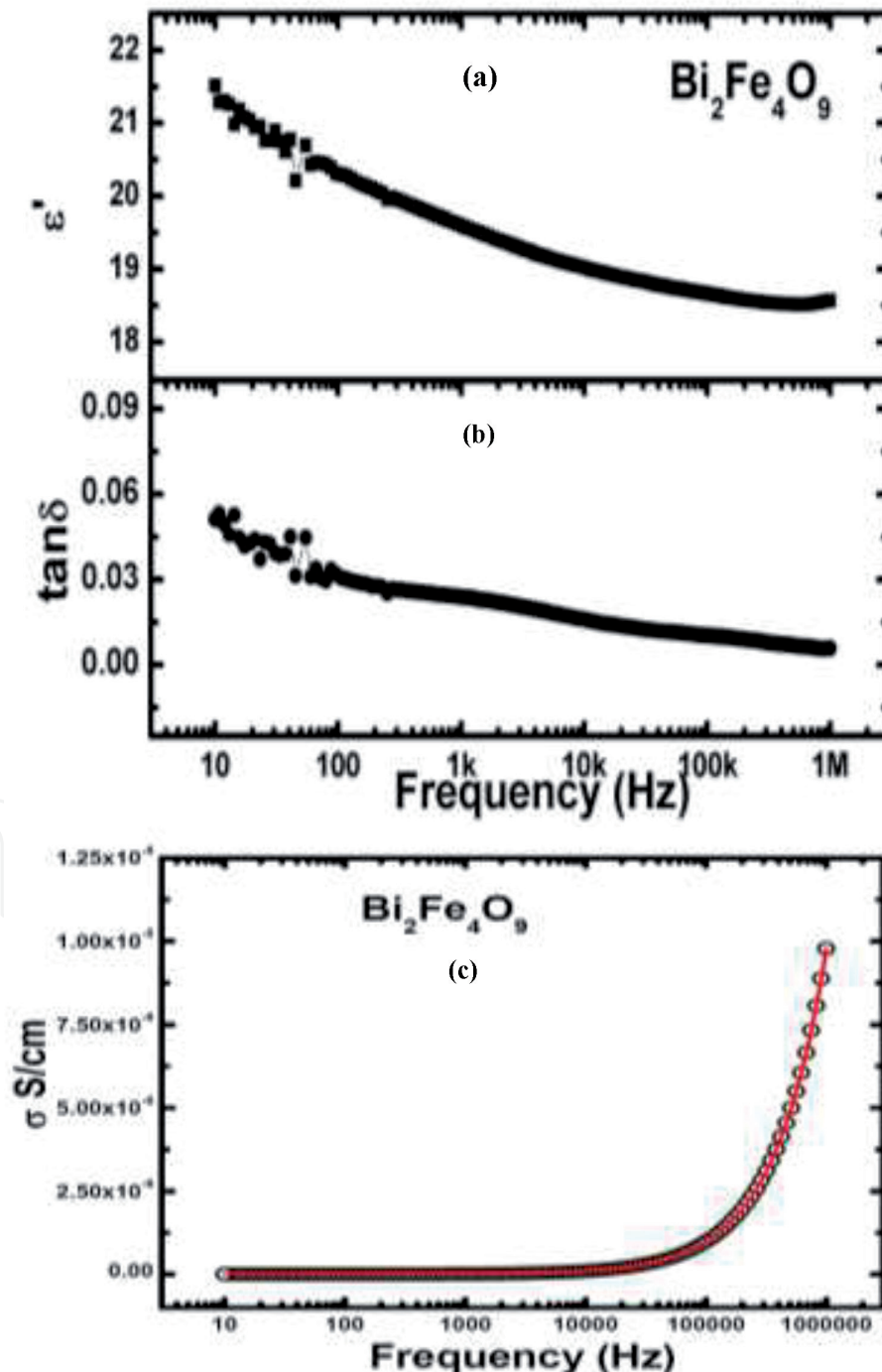**Figure 4.**
(a) Dielectric constant, (b) dielectric loss, and (c) frequency-dependent conductivity of $Bi_2Fe_4O_9$ ceramic.

ε' and tanδ are 18.59 and 0.006, respectively. Dielectric behavior (i.e. ε' and tanδ) decreases with increase in frequency and it is constant at higher frequency region. From **Figure 4(a)** and **(b)** we have found that the value of dielectric constant in the whole frequency range (10 Hz–1 MHz) is nearly constant representing the low loss in the prepared ceramic. This result appears to be consistent with previous empirical analysis using the Maxwell-Wagner model with thermal activation across multiple band gaps in isolated impurities [15, 33]. **Figure 4(c)** shows the semilog plot of conductivity (σ) at room temperature with frequency. The study of the frequency
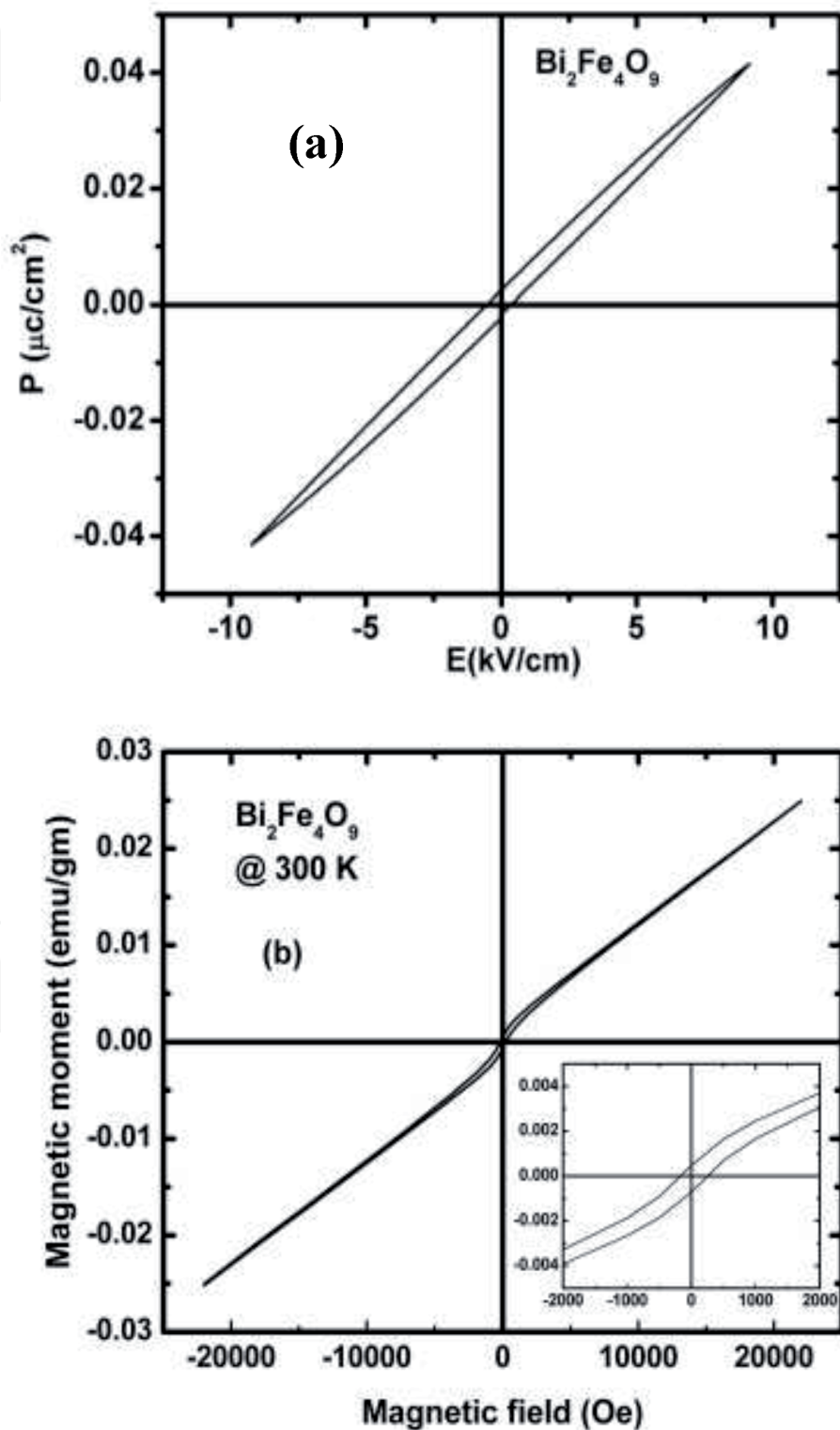

Figure 5.
(a) Polarization hysteresis P-E loop and (b) field-dependent magnetic hysteresis loop of Bi₂Fe₄O₉ ceramic at room temperature.

dependence of the conductivity is a deep-rooted method for describing the hopping dynamics of the charge carrier. The conductivity plot exhibits both low and high frequency dispersion phenomena [34–37]. The low-frequency region corresponds to the *dc* conductivity (σ_{dc}), which is due to the band conduction, and it is frequency independent. The high-frequency region corresponds to the *ac* conductivity (σ_{ac}), which is frequency dependent. To conclude, the electrical conductivity σ for $Bi_2Fe_4O_9$ follows the Jonscher power law [37]: $\sigma_{ac}(\omega) = \sigma_{dc} + A(T)\omega^n$. Here, A is the pre exponential factor and n is the power law exponent. The exponent n can have a value between 0 and 1. This parameter is frequency independent but temperature and material dependent.

Ferroelectric hysteresis $P(E)$ loop of the $Bi_2Fe_4O_9$ ceramic at room temperature represented in **Figure 5(a)**. The obtained loop indicates that there are ferroelectric properties with finite remanent polarization with the applied electric field in the prepared sample. Under an electric field of up to 10 kV/cm, the remanent polarization ($2P_r$) of $Bi_2Fe_4O_9$ was found to be 0.006 μC/cm^2. The observed polarization values are closely consistent with literature results [38].

3.5 Magnetic analysis (*M-H* curve)

From the measured *M-H* loop of $Bi_2Fe_4O_9$ ceramic (**Figure 5(b)**), the magnetic parameters we obtained are remanent magnetization ($M_r = 4.37 \times 10^{-4}$ emu/g), coercivity ($H_c = 239.4$ Oe) and saturation magnetization ($M_s = 0.024$ emu/g). In our $Bi_2Fe_4O_9$ ceramic, antiferromagnetic (AFM) and weak ferromagnetic (WFM) interactions exist simultaneously are consistent with the data reported earlier [15, 38–40]. The WFM order can be seen in the low magnetic field region. WFM order itself can be understood as a result of canted spin arrangements in two sublattices [41]. As the magnetic field increases, the ferromagnetic order saturates and the antiferromagnetic component dominates. There is even no sign of saturation. Obviously, in the prepared ceramic, M_r and M_s have achieved a non-zero value. We may note that the measured hysteresis curve confirm that the relationship between the applied magnetic field and the magnetization does not evidence of a linear behavior and shows the WFM. In the future, we can improve the magnetic and electric properties of $Bi_2Fe_4O_9$ ceramics with the appropriate doping or preparation techniques.

4. Conclusions

We have successfully synthesized polycrystalline $Bi_2Fe_4O_9$ through solid-state reaction route. X-ray diffraction pattern confirmed the formation of $Bi_2Fe_4O_9$ with the orthorhombic structure (space group *Pbam*). The obtained density of the present calcined $Bi_2Fe_4O_9$ ceramic is 6.51 g/cm^3. The room temperature Raman peak at 470 cm^{-1} is may be due to the magnetic origin of the material and might be related to magnon scattering. The value of the dielectric constant seems to be non-variable over the entire frequency range. It has been observed that the sample showed the presence of ferroelectricity. This study conclusively reported that a significant magnetic and ferroelectric order coexist in polycrystalline $Bi_2Fe_4O_9$ at room temperature. There is hysteresis in the electrical and magnetic curves, which proves the multiferroic nature of $Bi_2Fe_4O_9$ and making it more suitable for advanced technology and practical applications.

Conflicts of interest

All the authors declare that they have no conflict of interest.

Author details

Poorva Sharma[1*], Ashwini Kumar[1*], Jingyou Tang[1] and Guolong Tan[1,2]

1 Key Laboratory of Multifunctional Materials, Department of Electronic Engineering, Luzhou Vocational and Technical College, Luzhou, Sichuan, China

2 Institute of New Materials, Wuhan University of Technology, Wuhan, China

*Address all correspondence to: poorva@nuaa.edu.cn and 101101216@seu.edu.cn

IntechOpen

References

[1] Schmid H. Some symmetry aspects of ferroics and single phase multiferroics. Journal of Physics. Condensed Matter. 2008;**20**:434201

[2] Roni P. The Perovskite Handbook. Israel: Metalgrass Ltd; 2018. p. 108

[3] Park T-J, Papaefthymiou GC, Moodenbaugh AR, Mao Y, Wong SS. Synthesis, and characterization of submicron single-crystalline $Bi_2Fe_4O_9$ cubes. Journal of Materials Chemistry. 2005;**15**:2099-2105

[4] Liu H, Li L, Guo C, Ning J, Zhong Y, Hu Y. Thickness-dependent carrier separation in $Bi_2Fe_4O_9$ nanoplates with enhanced photocatalytic water oxidation. Chemical Engineering Journal. 2020;**385**:123929

[5] Yang H, Dai J, Wang L, Lin Y, Wang F, Kang P. A novel approach to prepare $Bi_2Fe_4O_9$ flower-like spheres with enhanced photocatalytic performance. Scientific Reports. 2017;7:768

[6] Poghossian AS, Abovian HV, Avakian PB, Mkrtchian SH, Haroutunian VM. Bismuth ferrites: New materials for semiconductor gas sensors. Sensors and Actuators B: Chemical. 1991;**4**:545

[7] Shamir N, Gurewitz E. The magnetic structure of $Bi_2Fe_4O_9$ – analysis of neutron diffraction measurements. Acta Crystallographica. Section A. 1978;**34**:662

[8] Niizeki N, Wachi M, Fur Z. The crystal structures of $Bi_2Mn_4O_{10}$, $Bi_2Al_4O_9$ and $Bi_2Fe_4O_9$. Kristallografiya. 1968;**127**:173-187

[9] Iliev MN, Litvinchuk AP, Hadjiev VG, Gospodinov MM, Skumryev V, Ressouche E. Phonon and magnon scattering of antiferromagnetic $Bi_2Fe_4O_9$. Physical Review B. 2010;**81**:024302

[10] Singh AK, Kaushik SD, Kumar B, Mishra PK, Venimadhav A, Siruguri V, et al. Substantial magnetoelectric coupling near room temperature in $Bi_2Fe_4O_9$. Applied Physics Letters. 2008;**92**:132910

[11] Verma A, Goel TC, Mendiratta RG, Alam MI. Dielectric properties of NiZn ferrites prepared by the citrate precursor method. Materials Science and Engineering B. 1999;**60**:156

[12] Rao SK, Abhinav EM, Jaison D, Sundararaj A, Santhiya M, Althaf R, et al. Investigation of room temperature multi-functional properties of Nd doped mullite $Bi_2Fe_4O_9$. Vacuum. 2020;**172**:109109

[13] Ameer S, Jindal K, Tomar M, Jha PK, Gupta V. Insight into electronic, magnetic, and optical properties of magnetically ordered $Bi_2Fe_4O_9$. Journal of Magnetism and Magnetic Materials. 2019;**475**:695

[14] Ameer S, Jindal K, Tomar M, Jha PK, Gupta V. Tunable electronic and magnetic properties of 3d transition metal doped $Bi_2Fe_4O_9$. Journal of Magnetism and Magnetic Materials. 2020;**509**:166893

[15] Pooladi M, Shokrollahi H, Lavasani SANH, Yang H. Investigation of the structural, magnetic, and dielectric properties of Mn-doped $Bi_2Fe_4O_9$ produced by reverse chemical co-precipitation. Materials Chemistry and Physics. 2019;**229**:39-48

[16] Moghadam AK, Mirzaee O, Shokrollahi H, Lavasani SANH. Magnetic and morphological characterization of bulk $Bi_2Fe_4O_9$ derived by reverse chemical co-precipitation: A comparative study of different sintering

methods. Ceramics International. 2019;**45**:8087-8094

[17] Zdorovets MV, Kozlovskiy AL. Study of phase transformations in Co/CoCo$_2$O$_4$ nanowires. Journal of Alloys and Compounds. 2020;**815**:152450

[18] Kozlovskiy AL, Kenzhina IE, Zdorovets MV. FeCo– Fe$_2$CoO$_4$/Co$_3$O$_4$ nanocomposites: Phase transformations as a result of thermal annealing and practical application in catalysis. Ceramics International. 2020;**46**:10262-10269

[19] Rusakov VS, Kadyzhanov KK, Kozlovskiy AL, Fadeev MS, Zdorovets MV. Phase transformations as a result of thermal annealing of nanocomposite Fe–Ni/Fe–Ni–O particles. Ceramics International. 2020;**46**:1586-1595

[20] Kozlovskiy A, Kenzhina I, Zdorovets M. Synthesis, phase composition and magnetic properties of double perovskites of A(FeM)O4-x type (A=Ce; M=Ti). Ceramics International. 2019;**45**:8669-8676

[21] Kozlovskiy A, Dukenbayevd K, Kenzhinaa I, Tosid D, Zdorovetsa M. Dynamics of changes in structural properties of AlN ceramics after Xe+22 ion irradiation. Vacuum. 2018;**155**:412

[22] Rodriguez-Carvajal J. Recent advances in magnetic structure determination by neutron powder diffraction. Physica B. 1993;**192**:55

[23] Zdorovets MV, Kozlovskiy AL. The effect of lithium doping on the ferroelectric properties of LST ceramics. Ceramics International. 2020;**45**:14548-14557

[24] Cai D, Du D, Yu S, Cheng J. Oriented growth of Bi$_2$Fe$_4$O$_9$ crystal and its photocatalytic activity. Procedia Engineering. 2012;**27**:577-582

[25] Tian ZM, Qiu Y, Yuan SL, Wu MS, Huo SX, Duan HN. Enhanced multiferroic properties in Ti-doped Bi$_2$Fe$_4$O$_9$ ceramics. Journal of Applied Physics. 2010;**108**:064110

[26] Bell AT. The impact of nanoscience on heterogeneous catalysis. Science. 2003;**299**:1688

[27] Liu ZS, Wu BT, Yin DG, Zhu YB, Wang LG. Enhanced photocatalytic activity in Al-substituted Bi$_2$Fe$_4$O$_9$ submicrocrystals. Journal of Materials Science. 2012;**47**:6777-6783

[28] Friedrich A, Biehler J, Morgenroth W, Wiehl L, Winkler B, Hanfland M, et al. High-pressure phase transition of Bi$_2$Fe$_4$O$_9$. Journal of Physics: Condensed Matter. 2012;**24**:145401

[29] Massey MJ, Baier U, Merlin R, Weber WH. Effects of pressure and isotopic substitution on the Raman spectrum of α-Fe$_2$O$_3$: Identification of two-magnon scattering. Physical Review B. 1990;**41**:7822

[30] Litvinchuk AP, Börjesson L, Thomsen C, Chu CW. Magnetic excitations in PrBa$_2$Cu$_4$O$_8$ explored by raman scattering. Physica Status Solidi B: Basic Solid State Physics. 1999;**215**:507

[31] Holmlund J, Knee CS, Andreasson J, Granath M, Litvinchuk AP, Börjesson L. Two-magnon Raman scattering from the Cu$_3$O$_4$ layers in (Sr$_2$, Ba$_2$) Cu$_3$O$_4$Cl$_2$. Physical Review B. 2009;**79**:085109

[32] White RM, Nemanich RJ, Herring C. Light scattering from magnetic excitations in orthoferrites. Physical Review B. 1982;**25**:1822

[33] Park YA, Song KM, Hur N. Frequency-Dependent dielectric anomalies in magnetic oxides. Journal of the Korean Physical Society. 2008;**53**:3356

[34] Shukla A, Choudhary RNP. Study of electrical properties of La^{3+}/Mn^{4+}-modified $PbTiO_3$ nanoceramics. Journal of Materials Science. 2012;**47**:5074

[35] Yamazaki Y, Satou M. High frequency conductivity in Cobalt-Iron ferrite. Japanese Journal of Applied Physics. 1973;**12**:998-1000

[36] Jonscher AK. Dielectric relaxation in solids. Journal of Physics D: Applied Physics. 1996;**32**:R57

[37] El Hiti MA. AC electrical conductivity of Ni-Mg ferrites. Journal of Physics D: Applied Physics. 1996;**29**:501-505

[38] Panda A, Govindaraj R, Amarendra G. Magneto dielectric coupling in $Bi_2Fe_4O_9$. Physica B: Condensed Matter. 2019;**570**:206-208

[39] Yuan X, Shi L, Zhao J, Zhou S, Guo J. Tunability of magnetization and bandgap in mullite-type $Bi_2Fe_4O_9$ ceramics through non-magnetic ions. Scripta Materialia. 2018;**146**:55-59

[40] Liu T, Xu Y, Zeng C. Synthesis of $Bi_2Fe_4O_9$ via PVA sol–gel route. Materials Science and Engineering B. 2011;**176**:535-539

[41] Dormann JL, Nogues M. Magnetic structures in substituted ferrites. Journal of Physics: Condensed Matter. 1990;**2**:1223